frontiers | Frontiers in Energy Research

ORIGINAL RESEARCH
published: 13 May 2022
doi: 10.3389/fenrg.2022.903514

Energy and Exergy Analysis on a Novel Solar-Air Dual-Source Vapor Injection Heat Pump Air-Conditioner for the Electric Bus

Hong Zhang[1]*, *Qian Liu*[2] and *Lichen Yang*[2]

[1]Automobile Institute, Henan College of Transportation, Zhengzhou, China, [2]Yutong Bus Co., Ltd., Zhengzhou, China

A novel solar-air dual-source vapor injection heat pump air-conditioner for the electric bus is proposed, aiming to enhance the system heating performance and increase the vehicle endurance. Three working modes are designed for the proposed system, including solar-air dual-source heating mode, air source heating mode, and cooling mode. The system heating performance is explored by the simulation approach. Compared with the conventional vapor injection heat pump, the proposed system averagely enlarges the heating capacity and efficiency by 17.0% and 21.2%, respectively, under the considered evaporating temperature range (–25~0°C) by utilizing the solar energy. Moreover, the two systems possess the optimal intermediate pressures to achieve the maximal heating efficiency. The system performance comparison under the two heating modes indicates that the dual-source mode is preferred except for the extremely low or no solar radiation situation. The exergy analysis shows that more than half of the system total exergy input is destructed in the solar collector, which grows by 111.4% as the solar radiation intensity increases by 300 W m^{-2}; thus, the system exergy efficiency decreases as the solar radiation enhances, although the system heat exergy output shows a growth tendency. The component irreversibility analysis on the proposed system is also conducted, aiming to explore the reason for the system exergy performance variation and the irreversibility distribution rule. At last, the exergy flow situations of the proposed system and the conventional system are contrastively analyzed. The exergy performance comparison indicates that under the given condition the proposed system can improve the exergy output by 20.2% and decrease the electricity consumption by 4.5% compared with the conventional system.

Keywords: solar-air dual-source, heat pump, vapor injection, exergy analysis, energy analysis

OPEN ACCESS

Edited by:
Guojie Zhang,
Zhengzhou University, China

Reviewed by:
Yuanyuan Zhou,
Nanjing University of Science and Technology, China
Rijing Zhao,
Xi'an Jiaotong University, China

***Correspondence:**
Hong Zhang
hzhang_hncc@yeah.net

Specialty section:
This article was submitted to Process and Energy Systems Engineering, a section of the journal Frontiers in Energy Research

Received: *24 March 2022*
Accepted: *13 April 2022*
Published: *13 May 2022*

Citation:
Zhang H, Liu Q and Yang L (2022) Energy and Exergy Analysis on a Novel Solar-Air Dual-Source Vapor Injection Heat Pump Air-Conditioner for the Electric Bus. Front. Energy Res. 10:903514. doi: 10.3389/fenrg.2022.903514

INTRODUCTION

Aiming to reduce the greenhouse gas emission and go carbon neutral, the Chinese government makes great efforts to promote the vehicle electrification (Xiao et al., 2020). For the electric vehicle, the traditional single-cold air-conditioner system needs to be modified for realizing heating performance, due to the absence of the waste heat from the engine (Peng and Du, 2016). In the initial stage, the PTC (positive temperature coefficient) heater is added to the electric vehicle air-conditioner and provides thermal heat by directly converting electricity into heat. However, the

heating efficiency of this electric resistance heater is always less than 1 and seriously degrades the vehicle endurance mileage. A relevant study indicated that the endurance mileage of the electric passenger vehicles could produce up to 45% reduction when adopting the PTC heater to heat under the ambient temperature of 0°C (Göhlich et al., 2015). Therefore, benefiting from the improvement of the industrial chain, the heat pump air-conditioner with higher heating efficiency gradually becomes the mainstream in electric vehicles. Various research studies have been conducted on the operation characteristics and optimization research into the heat pump air-conditioner for electric vehicles (Zhang et al., 2018). Fazhan et al. (2014) experimentally investigated the variation tendency of the heating performance of the vehicle heat pump air-conditioner with the ambient temperature. Li et al. (2016) proposed a heat pump air-conditioner for electric vehicles with R134a and obtained a heating COP (coefficient of performance) of 2.3 under the ambient temperature of 5°C. However, the traditional single-stage heat pump system owns an inherent disadvantage that its heating performance degrades seriously under cold environment conditions (Wei et al., 2020). Thus, massive efforts have been made to improve the low-temperature adaptation of the vehicle heat pump air-conditioner, including structure modification (Feng and Hrnjak, 2016), refrigerant substitution (Llopis et al., 2015; Wang et al., 2016), and component optimization (Zhang et al., 2019).

Numerous studies have proved that the vapor injection technology possessed the potential to improve the heating performance of the heat pump system, especially under low-temperature ambient conditions (Wang et al., 2021). Through quasi-secondary compression, the vapor injection heat pump can realize greater heating efficiency, longer compressor life, and easier capacity adjustment (Li et al., 2020). The application research on this technique in the vehicle air-conditioner is the hotspot in recent years. Li et al. (2014) experimentally investigated a vapor injection air-source heat pump for electric vehicles and declared that the heating capacity and COP were, respectively, improved by 28% and 70% over those of the baseline system. Kwon et al. (2017) compared the performance of the non-injection heat pump and economizer vapor injection heat pump and declared that the latter one produced 14%~44% heating capacity improvement under the driving condition. Han et al. (2019) developed a vapor injection air-source heat pump for electric buses and achieved 14.5% heating COP improvement over the non-injection system under the working condition of −20/20°C. Summarily, previous research studies have strongly proved that it may be a promising way to improve the poor low-temperature adaptation of the vehicle heat pump air-conditioner by adopting the vapor injection technology.

Except for the vapor injection technique, utilizing solar energy is also an effective method to improve the heat pump performance in cold regions. In fact, vast research works on solar energy utilization in the air-source heat pump system already exist. Chen and Yu (2018) proposed a solar-assisted vapor injection heat pump with a subcooler and then declared obvious heating performance enhancement based on the simulation results. Besagni et al. (2019) proposed a novel solar-air dual-source multifunctional heat pump and improved the heating COP by 34% over the air-source system. Cai et al. (2020) also presented a solar-air dual-source heat pump and then achieved a heating COP of up to 4.58 under the given condition. From these research studies, it can be concluded that both the vapor injection technique and solar energy utilization technique own the potentials to improve the heat pump performance, and combining the two techniques together should produce more outstanding effect. Nevertheless, utilizing solar energy in the light-duty vehicle faces the difficulty that the installation of the solar collector may destruct the vehicle aesthetically and increase the windage resistance. This severely restricts the application of the solar energy utilization technique in the electric vehicle. Fortunately, the electric bus does not have this problem, which owns a big and flat roof for solar collector installation. Moreover, the electric bus mainly runs during daytime on uncovered roads, which is beneficial to the solar energy absorption. Therefore, solar energy utilization should be a feasible way to enhance the heating performance of the electric bus air-conditioner and increase the vehicle endurance.

Based on the aforementioned analysis, a novel solar-air dual-source vapor injection heat pump air-conditioner for the electric bus is proposed, driven by the desire to improve the heating performance of the vehicle air-conditioner by utilizing solar energy. The energetic and exergy performance of this proposed system will be carried out by the simulation method. The research can provide a fundamental data reference for the research and application of this proposed system in future.

SYSTEM DESCRIPTION

The cycle structure of this novel solar-air dual-source vapor injection heat pump air-conditioner for the electric bus (DS-VIHP) is illustrated in **Figure 1**, which includes twelve devices: a vapor injection compressor, a four-way valve, an indoor heat exchanger, two expansion valves, a separator, a solar collector, a mixer, an outdoor heat exchanger, a globe valve, and two check valves. The DS-VIHP system owns three working modes: solar-air dual-source heating mode (DS mode), air source heating mode (AS mode), and cooling mode. The working modes of the DS-VIHP system can be switched by controlling the globe valve and four-way valve. The four-way valve owns two modes: mode A (port a connects port b, and port c connects port d) and mode B (port a connects port d, and port c connects port b).

As shown in **Figure 1A**, this proposed system works at the solar-air dual-source heating mode (DS mode) when the globe valve is opened and the four-way valve stays at mode A. The high-pressure superheated vapor (state 2) enters the indoor heat exchanger (works as a condenser) and then becomes subcooling liquid (state 3) after releasing thermal heat into the cabin. This liquid at state 3 expands to be medium-pressure two-phase fluid (state 4), after flowing through the expansion valve I, and then separates the gas and the liquid in the separator. The saturated liquid (state 6) leaving the separator divides into two branches. The

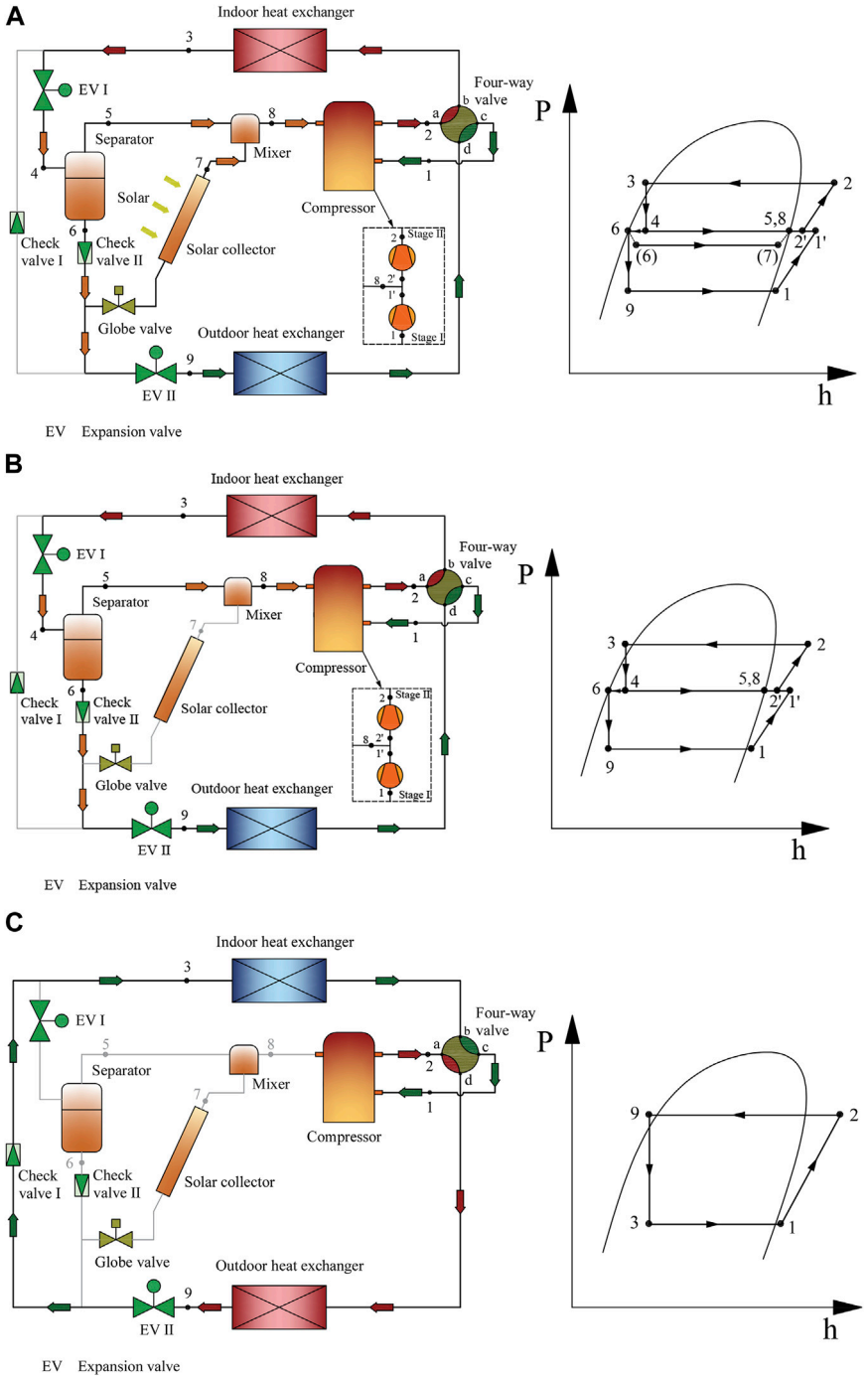

FIGURE 1 | Schematic and P-h diagrams of three working modes for the DS-VIHP system: DS mode **(A)**, AS mode, **(B)** and cooling mode **(C)**.

saturated liquid in the main branch expands in the expansion valve II and becomes the two-phase refrigerant (state 9), which further completely evaporates in the outdoor heat exchanger (works as an evaporator). The superheated vapor (state 1) leaving the outdoor heat exchanger is eventually suctioned into the compressor suction port. The saturated liquid in the bypass branch enters the solar collector and evaporates to be refrigerant vapor (state 7) after absorbing solar energy. This vapor (state 7) mixes with the saturated vapor (state 5) from the separator in the mixer and then enters the compressor injection port. By comparing **Figures 1A,B**, it can be found that the only difference between the air-source heating mode and the DS mode is the absence of a bypass branch. Under the AS mode, the globe

valve closes, and no refrigerant flows through the solar collector to absorb solar energy.

When the cabin needs cooling, the proposed system works at the cooling mode by switching the four-way valve to mode B and closing the globe valve and expansion valve I, as shown in **Figure 1C**. The high-pressure superheated vapor (state 2) enters the outdoor heat exchanger (works as a condenser) and becomes a subcooling liquid (state 9) after releasing thermal heat to the ambient. This liquid (state 9) becomes a two-phase flow (state 3) after flowing through the expansion valve II. This two-phase flow at state 3 completely evaporates in the indoor heat exchanger (works as an evaporator) after absorbing thermal heat from the cabin and eventually returns to the compressor suction port.

MATHEMATICAL MODEL

It should be pointed out that only the mathematical model for the DS mode of the DS-VIHP system will be presented in the following content, aiming to keep the content concise. In fact, the mathematical models for the AS mode and cooling mode have been presented in various literature works (Choi et al., 2017; Kim et al., 2018). Moreover, the system performance under the cooling mode will not be explored in this analysis because it is just a classical single-stage vapor compression refrigeration cycle.

Energy Model

The energy model for the DS mode of the DS-VIHP system is built based on the first thermodynamics law, aiming to evaluate its energetic performance. Also, the compressor power input can be calculated by:

$$W_{com} = m_1 (h_{1s} - h_1) + m_2 (h_2 - h_{2s}), \tag{1}$$

where m_1 and m_2 are the refrigerant mass flow rates in the stage I and II compression processes, respectively, h_1 and h_{2s} are the initial refrigerant-specific enthalpies of the stage I and II compression processes, respectively, and h_{1s} and h_2 are the final refrigerant specific enthalpies of the stage I and II compression processes, respectively; h_{1s} can be calculated by the following equation:

$$h_{1s} = h_1 + \frac{h_{1s,is} - h_1}{\eta_{is}}, \tag{2}$$

where $h_{1s,is}$ is the hypothesis refrigerant-specific enthalpy after an isentropic stage I compression process, and η_{is} represents the isentropic efficiency of the compression process and is regarded as (Chen and Yu, 2018):

$$\eta_{is} = 0.874 - 0.0135 \frac{P_2}{P_1}. \tag{3}$$

The final refrigerant specific enthalpy after the second compression process can be calculated by:

$$h_2 = h_{2s} + \frac{h_{2,is} - h_{2s}}{\eta_{is}}, \tag{4}$$

where $h_{2,is}$ is the hypothesis refrigerant-specific enthalpy after an isentropic stage II compression process. The refrigerant mixing process at the compressor injection port observes the following energy balance equation:

$$m_2 h_{2s} = m_1 h_{1s} + m_8 h_8, \tag{5}$$

where m_8 is the mass flow rate of the injection vapor entering the compressor vapor injection port.

$$m_8 + m_1 = m_2. \tag{6}$$

Defining the system injection ratio as follows:

$$\alpha = \frac{m_8}{m_2}. \tag{7}$$

The mass flow rate of the refrigerant vapor suctioned by the compressor from the evaporator can be calculated by the following equation:

$$m_1 = \frac{\eta_v n_{com} V_{dis} d_1}{60}, \tag{8}$$

where n_{com} represents the compressor rotational speed, V_{dis} is the compressor displacement volume, d_1 is the refrigerant density at the suction port, and η_v represents the volume efficiency (Chen and Yu, 2018).

$$\eta_v = 0.959 - 0.00642 \frac{P_2}{P_1}. \tag{9}$$

The solar energy is finally gained by the flat-plate collector with a double glazing glass, and the heat insulator can be obtained by the Hottel–Whillier–Bliss (HWB) equation (Diez et al., 2019).

$$Q_{gain} = \varepsilon_{pl} \tau_g A_{pl} G - U_{sc} A_{pl} (T_{pl} - T_{air}), \tag{10}$$

where G is the solar radiation intensity, A_{pl} is the solar absorber plate area in the solar collector, ε_{pl} is the absorption factor of the solar absorber plate, τ_g is the transmissivity of the glass cover, Usc is the heat loss coefficient of the solar collector to the environment, T_{pl} is the average temperature of the solar absorber plate, and T_{air} is the ambient air temperature.

The refrigerant through the solar collector observes the following energy balance equation:

$$Q_{gain} = m_7 (h_7 - h_6). \tag{11}$$

The system heating capacity and COP are expressed by:

$$Q_h = m_2 (h_2 - h_3), \tag{12}$$

$$COP_h = \frac{Q_h}{W_{com}}. \tag{13}$$

Exergy Model

The exergy analysis method is able to not only evaluate the secondary thermodynamic performance of an overall system but also examine the irreversibility of every system component. Based on the exergy analysis result, the component optimization priority can be obtained when carrying out the system modification; and then, the following exergy model for the

DS-VIHP system is built according to the second thermodynamics law.

As known, the refrigerant exergy at any point of a vapor compression system can be defined as (Qin et al., 2021):

$$Ex = m[(h - h_0) - T_0(s - s_0)]. \quad (14)$$

Here, T_0 and P_0 are the reference temperature and pressure, which are chosen as 298.15 K and 101.325 kPa, respectively, in this analysis.

The total exergy input of the DS-VIHP system can be calculated by:

$$Ex_{sys} = W_{com} + Ex_{rad}. \quad (15)$$

Ex_{solar} is the solar exergy input through absorbing solar energy.

$$Ex_{solar} = A_{pl}G\left(1 - \frac{T_{air}}{T_s}\right), \quad (16)$$

where T_s is the apparent Sun temperature and set at 4,500 K in this analysis (Jafarkazemi and Ahmadifard, 2013).

The exergy destruction (I_k) and exergy destruction percentage (φ_k) of the kth component in the DS-VIHP system are calculated by **Eqs 17–28**.

For the compressor,

$$I_{com} = (m_2 s_2 - m_1 s_1 - m_8 s_8)T_0, \quad (17)$$

$$\varphi_{com} = \frac{I_{com}}{Ex_{sys}}. \quad (18)$$

For the condenser,

$$I_{con} = m_2[h_2 - T_0 s_2 - (h_3 - T_0 s_3)] - Q_h\left[1 - \frac{T_0}{(T_c - \Delta T_c)}\right], \quad (19)$$

$$\varphi_{con} = \frac{I_{con}}{Ex_{sys}}, \quad (20)$$

where ΔT_c is the difference between the cabin temperature and the condensing temperature, which is assumed as 10 K in this analysis.

For the throttling valve I,

$$I_{tv1} = m_2(s_4 - s_3)T_0, \quad (21)$$

$$\varphi_{tv1} = \frac{I_{tv1}}{Ex_{sys}}. \quad (22)$$

For the solar collector,

$$I_{sc} = m_7[h_6 - T_0 s_6 - (h_7 - T_0 s_7)] + Ex_{rad}, \quad (23)$$

$$\varphi_{sc} = \frac{I_{sc}}{Ex_{sys}}. \quad (24)$$

For the throttling valve II,

$$I_{tv2} = m_1(s_9 - s_6)T_0. \quad (25)$$

$$\varphi_{tv2} = \frac{I_{tv2}}{Ex_{sys}}. \quad (26)$$

For the evaporator,

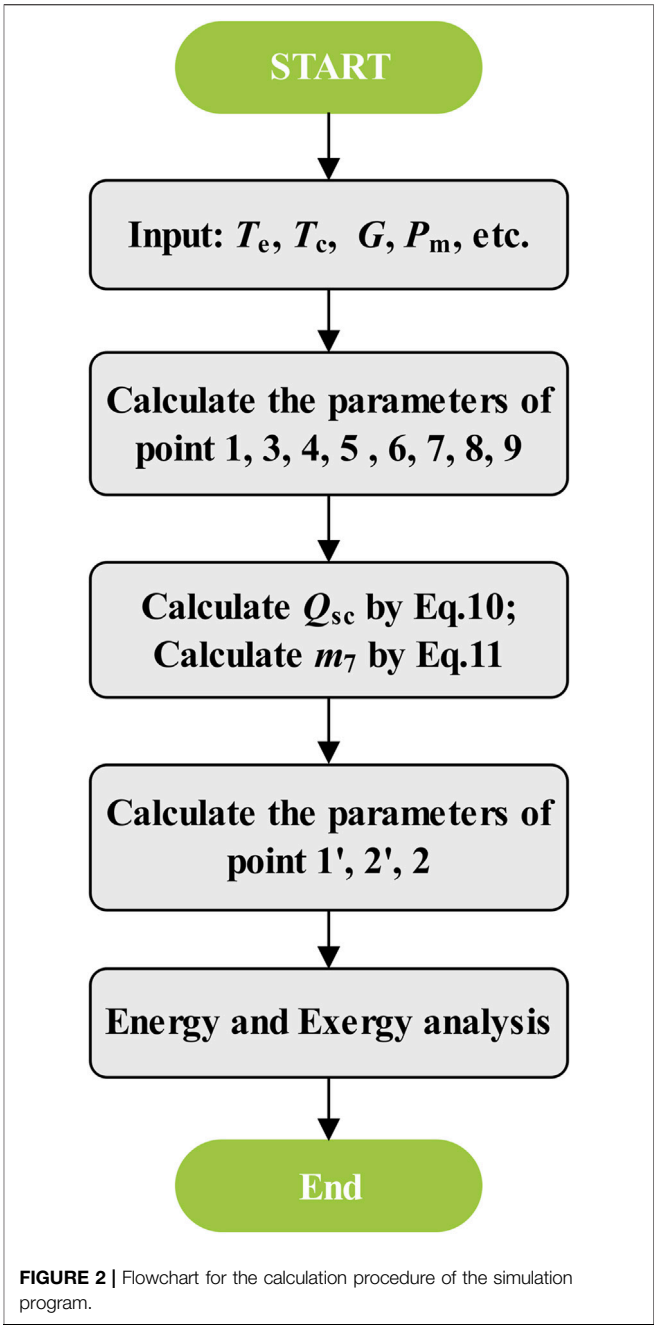

FIGURE 2 | Flowchart for the calculation procedure of the simulation program.

$$I_{eva} = m_1[h_9 - T_0 s_9 - (h_1 - T_0 s_1)], \quad (27)$$

$$\varphi_{eva} = \frac{I_{eva}}{Ex_{sys}}. \quad (28)$$

The heat exergy outputting from the condenser is:

$$Ex_h = Q_h\left[1 - \frac{T_0}{(T_c - \Delta T_c)}\right]. \quad (29)$$

The system exergy efficiency can be calculated by the following equation:

TABLE 1 | Necessary component parameters for the simulation program.

Device		Parameter
Solar collector	A_{pl}	5 m^2
	ε_{pl}	0.95
	τ_g	0.92
	U_{sc}	4.35 W m^{-2} K^{-1}
Compressor	V_{dis}	80 cm^{-3} r^{-1}
	n_{com}	2,800 r min^{-1}

TABLE 3 | Thermophysical parameters of R410A, R407C, R134a, and R1234yf.

Refrigerant	t_{crit} (°C)	P_{crit} (MPa)	NBP (°C)	GWP	Safety class
R410A	72.5	4.95	−51.6	1,730	A1
R407C	86.7	4.62	−43.6	1,700	A1
R134a	101.1	4.06	−26.1	1,430	A1
R1234yf	94.7	3.38	−29.5	4	A2L

TABLE 2 | Validation of the FVHP system model with the existing work.

Parameter	Present work	Existing work	Relative error (%)
Coefficient of performance, COP_h	3.717	3.739	−0.59
Heating capacity, Q_h (kW)	30.14	29.8	+1.14
Injection ratio, α	0.2595	0.261	−0.57
Discharge temperature, t_2 (°C)	116.3	115.7	+0.52

$$\eta_{exh} = \frac{Ex_h}{Ex_{sys}}. \tag{30}$$

It should be noted that the thermodynamic characteristics of the conventional flash tank vapor injection heat pump system (FVHP) will also be simulated for comparison, although its mathematical model is not presented for brevity. In the following content, the heating performance of the DS-VIHP system refers in particular to its heating performance under the dual-source mode, unless otherwise specified.

Model Solving Method and Validation

The energetic and exergy performance of the proposed DS-VIHP system and the FVHP system will be compared based on the aforementioned mathematical model. The system simulation program is written based on MATLAB software, and the solving procedure of the mathematical model of the DS-VIHP system is illustrated in **Figure 2**. In the simulation program, the refrigerant thermophysical parameter is obtained by invoking the property subroutines using REFPROP 10.0 (Lemmon et al., 2018). Based on the actual operation condition of the electric bus air-conditioner, the heating performance analysis will be carried out based on the following operation conditions: considered ranges of the evaporating temperature and condensing temperature are -25~0°C and 25~50°C, respectively, subcooling/superheat degrees of the refrigerant flowing out the condenser/evaporator are fixed at 5°C, the median value of the actual solar radiation intensity 600 W m^{-2} is selected unless otherwise specified, and the refrigerant flowing out of the solar collector is saturated vapor. Referring to previous research studies (Pridasawas and Lundqvist, 2004), **Table 1** displays the necessary component parameters for the simulation program.

To verify the aforementioned mathematical model, the simulation data from the developed program of the convenient FVHP system are compared with those reported by Redón et al. (2014) under the given condition (t_e = −8°C, t_c = 65°C, P_m = 1,833 kPa, and refrigerant = R32), as listed in **Table 2**. As shown, the maximum error of the six considered parameters between the present work and the existing work is less than 1.14%, that is, the FVHP system model possesses the satisfactory agreement. Thus, it can be concluded that the presented simulation mode of the DS-VIHP system should maintain high reliability, which is established by adding the HWB equation to the verified FVHP system model.

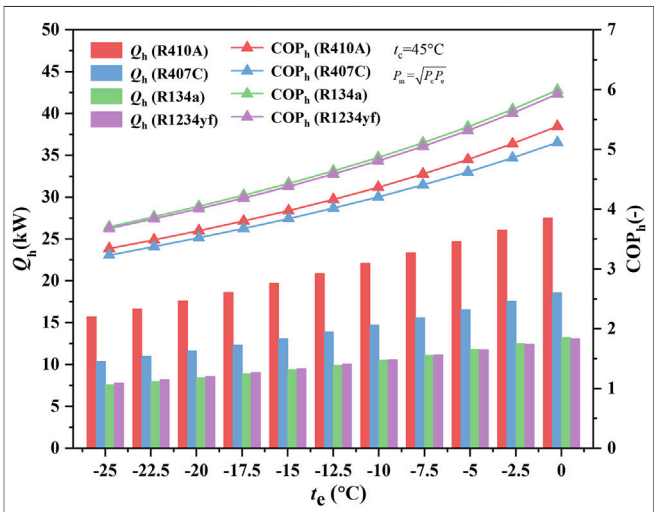

FIGURE 3 | Performance comparison of DS-VIHP with different refrigerants.

RESULTS AND DISCUSSION

As known, the refrigerant type is a key influence factor on the system performance, and thus the heating performance of the DS-VIHP system with four typical automobile air-conditioner refrigerants (R410A, R407C, R134a, and R1234yf) are

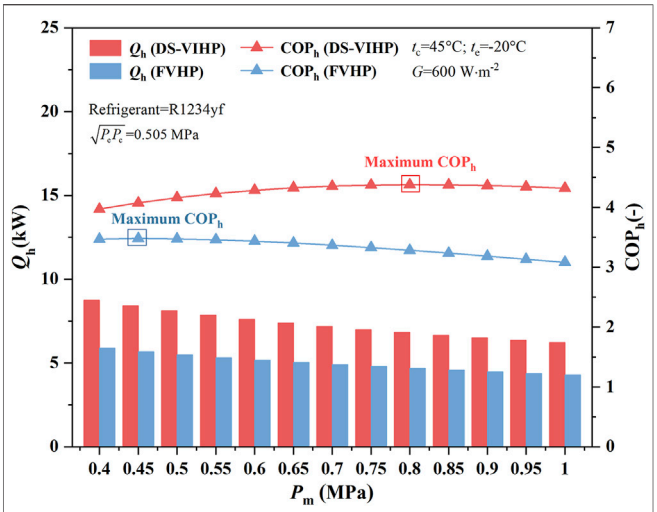

FIGURE 4 | Performance variations of two systems with the intermediate pressure.

compared based on the built model. The thermophysical parameters of the four refrigerants are listed in **Table 3**. The comparison of the system heating capacity (Q_h) and COP (COP_h) using these refrigerants under different evaporating temperatures (t_e, −25~0°C) are exhibited in **Figure 3**, when the condensing temperature (t_c) is set at 45°C. The system intermediate pressure (P_m) is set as the square root of the product of the condensing pressure (P_c) and evaporating pressure (P_e). As shown, R410A always obtains the maximal heating capacity, followed by R407C, R1234yf, and R134a. According to the simulation results, the system heating capacity using R410A is superior to that using R407C, R1234yf, and R134a by an average of 50.0%, 106.7% and 108.9%, respectively. Meanwhile, R410A averagely decreases the system heating COP by 10.1% and 9.2% compared with R134a and R1234yf, and improves the heating COP by 3.9% over the R407C. Although possessing excellent thermophysical properties, R134a is ongoing a phase-down process due to its high GWP (1301). Moreover, it can be seen that R1324yf produces almost identical heating capacity and COP to R134a, as an environmentally friendly substitution for the latter one. Based on the principle of heating efficiency maximization and environmental protection, R1234yf is chosen as the main work medium in the following analysis.

To evaluate the influence of the intermediate pressure on the heating performance of the two systems, the heating capacity and COP of the proposed DS-VIHP system and the FVHP system under different vapor intermediate pressures (P_m) are compared in **Figure 4**, while the condensing temperature and evaporating temperature were kept at 45°C and −20°C. Not surprisingly, the heating capacities of the two systems always drop down as the intermediate pressure improves. According to the simulation results, the heating capacities of the DS-VIHP system and the FVHP system are, respectively, decreased by 28.9% and 27.0%, as the intermediate pressure is lifted from 0.4 to 1.0 MPa. It is mainly ascribed to the refrigerant vapor quality reduction at the separator inlet as lifting the intermediate pressure, which further reduces the mass flow rate of the injection vapor. After that, fewer refrigerants will be discharged to the condenser, and then the system heating capacity will decrease. In addition, it can also be found that both the two systems own the optimal intermediate pressures to realize the maximal COP. As shown, the DS-VIHP system and the FVHP system, respectively, obtain the maximal COP around the intermediate pressures of 0.80 and 0.45 MPa. It indicates that the optimum intermediate pressure of the convenient FVHP system for the maximal heating COP is close to the square root of the product of condensing pressure and evaporating pressure (0.505 MPa), corresponding to the well-known conclusion. Except for evaporating and condensing pressures, the optimal intermediate pressure of the DS-VIHP system is also concerned with multiple other factors, including the solar radiation intensity, solar collector area, and refrigerant flow rate. In the following analysis, the optimal intermediate pressure for the maximal heating COP will be chosen as the working intermediate pressure, if not otherwise specified.

The heating capacity and COP of the DS-VIHP system under different evaporating temperatures are compared with those of the FVHP system in the **Figure 5**, aiming to evaluate its heating performance advantage. The condensing temperature is kept at 45°C, while the evaporating temperature ranges between −25°C and 0°C. As expected, the heating performance of the DS-VIHP system always exceeds that of the FVHP system under the given condition. Actually, as the evaporating temperature grows from −25°C to 0°C, the DS-VIHP system, respectively, increases the heating capacity and COP by 23.2%~12.0%, and 30.4%~14.2% over the FVHP system. It is because absorbing the solar energy can raise the dryness of the two-phase refrigerant entering the separator, which further increases the injection vapor flow rate and enhances the heating performance. In addition, it also implies that the superiority of the DS-VIHP system is enhanced as the evaporating temperature drops down. It is because the air energy absorbed by the evaporator from the ambient reduces by lowering

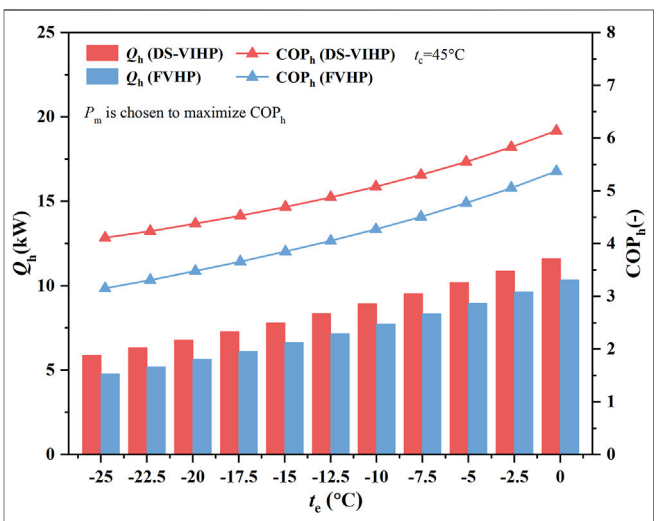

FIGURE 5 | Performance comparison under different evaporating temperatures.

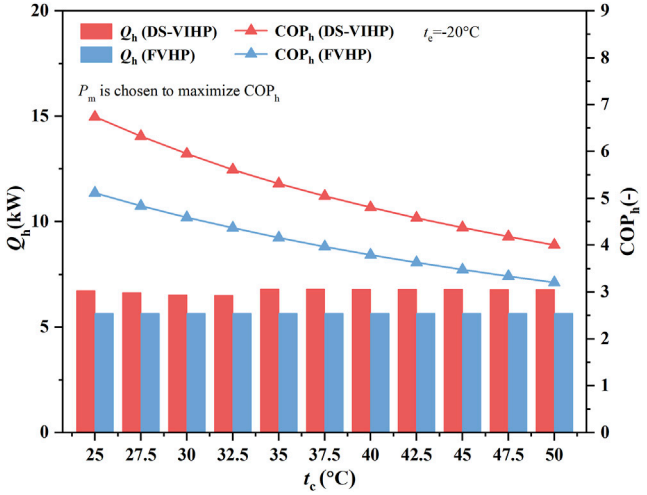

FIGURE 6 | Performance comparison under different condensing temperatures.

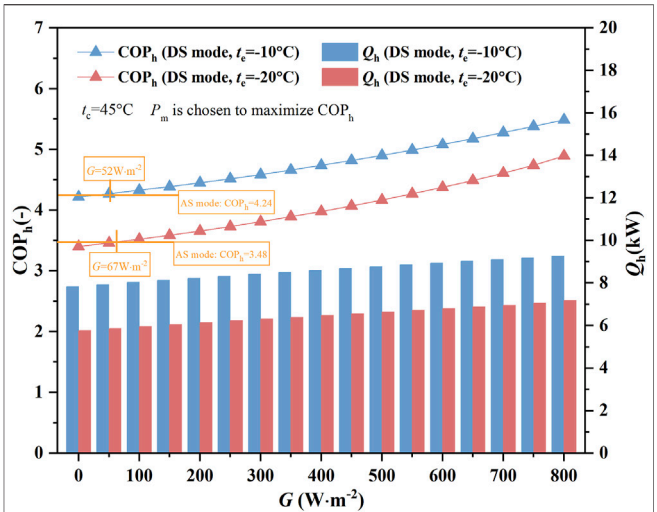

FIGURE 7 | Performance comparison under different solar radiations.

the evaporating temperature, and then the performance improvement effect of utilizing solar energy is enhanced because the absorbed solar energy has shown a little change.

The heating performance comparison of the DS-VIHP system and the FVHP systems under different condensing temperatures is displayed in **Figure 6**, when the evaporating temperature is fixed at −20°C. Similar to the situation in **Figure 5**, the DS-VIHP system outperforms the FVHP system throughout the condensing temperature scope. As the condensing temperature ranges between 25°C and 50°C, the DS-VIHP system, respectively, exceeds the FVHP system in the heating capacity and COP aspects by an average of 19.1% and 27.7%. In line with the expectation, the heating COP of the two systems dramatically decreases by lifting the condensing temperature, while their heating capacities yield a relatively flat variation tendency. Actually, as the condensing temperature rises from 25°C to 50°C, the heating COP of the DS-VIHP system and the FVHP system, respectively, decreases by 40.5% and 37.4%, while the maximal variation range of the heating capacity is less than 2%. In summary, the proposed DS-VIHP system yields more significant heating capacity and COP over the convenient FVHP by utilizing solar energy under all the considered operation conditions.

The heating performance variation tendencies of the DS-VIHP system with the solar radiation intensity (G) under the DS mode and the AS mode are displayed in **Figure 7**, when the condensing temperature is 45°C. As shown, both the heating capacity and COP grow up with strengthening the solar radiation, in line with expectations. Actually, as G rises from 0 W m^{-2} to 800 W m^{-2}, the heating COP grows up from 4.22 to 5.49 at the evaporating temperature of −10°C and 3.40 to 4.90 at the evaporating temperature of −20°C. Meanwhile, the FVHP system yields constant COP values of 4.24 and 3.48 at the evaporating temperatures of −10°C and −20°C, respectively. A similar situation occurs in the system heating capacity comparison. It can be seen from **Figure 7** that the DS mode can help the DS-VIHP system obtain superior heating performance when the solar radiation intensity exceeds 52 W m^{-2} for the evaporating temperature of −10°C and 67 W m^{-2} for the evaporating temperature of −20°C. This demonstrates that the DS mode is suitable for the proposed DS-VIHP system except under the very low and no solar radiation cases. This phenomenon is mainly ascribed to that the heat transferring to the refrigerant from the solar collector equals the difference between the solar energy radiated on the collector surface and the heat leaked to the surrounding. Under the very low or no Sun radiation situation, the refrigerant loses heat to the surrounding and degrades the heating performance. In other cases, the solar collector eventually transfers heat to the refrigerant in the solar collector and then contributes to the performance superiority under the DS mode. In addition, it also can explain why the DS-VIHP system offers two heating modes depending on the solar radiation condition.

The variation tendencies of the compressor input work (W_{com}), solar exergy input (Ex_{solar}), heat exergy output (Ex_h), and exergy efficiency (η_{exh}) of the DS-VIHP system with the solar radiation intensity are illustrated in the **Figure 8**, aiming to examine the system irreversibility. The condensing temperature is set at 45°C, when the evaporating temperature is −10°C and −20°C. As shown, the heat exergy output always grows up as it strengthens the Sun radiation, although the heat exergy efficiency yields an opposing situation. Actually, as G rises from 100 to 800 W m^{-2}, the exergy output grows up by 15.5% (260.6–300.9 W) at the evaporating temperature of −10°C, while the exergy efficiency relatively drops down by 46.7%. It is ascribed to that the total exergy input leads to a more significant improvement against the exergy output as it enhances the solar radiation. As G increases by 700 W m^{-2}, the system's overall exergy input is increased up to 116.7% (2,049.8–4,442.4 W) at the evaporating temperature of −10°C. Thus, the variation tendency of the system exergy efficiency is contrary to that of the available heat exergy output. In addition,

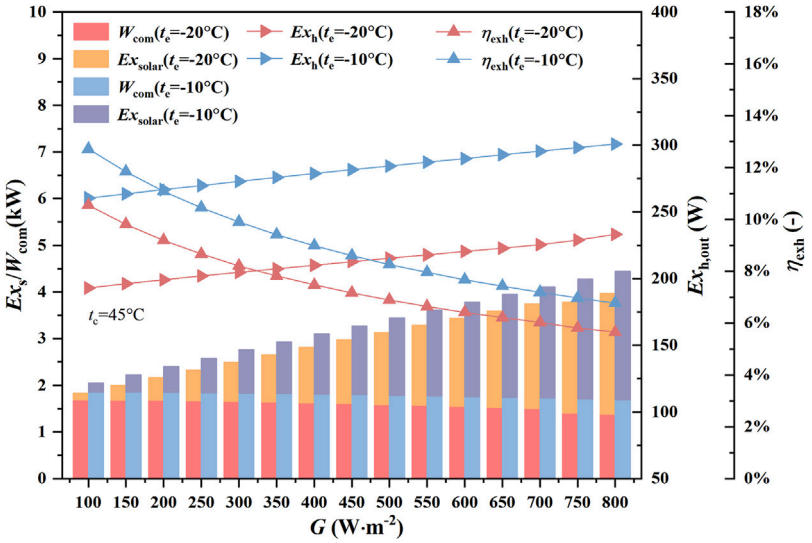

FIGURE 8 | Variation of system exergy performance with solar radiation intensity.

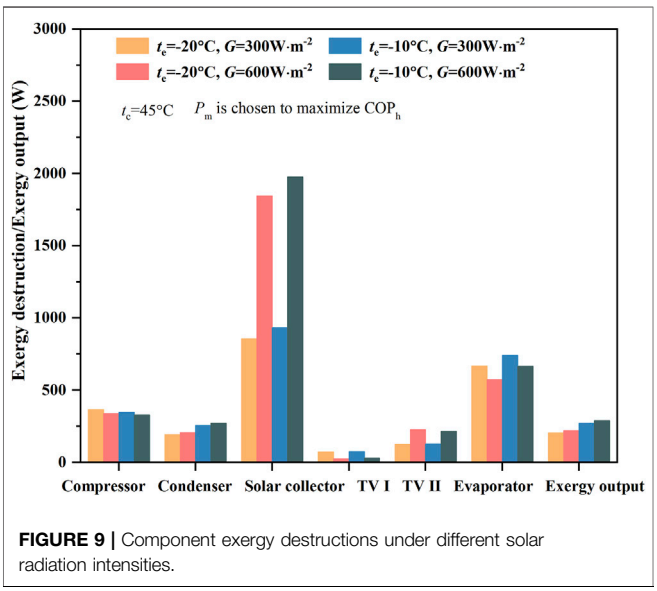

FIGURE 9 | Component exergy destructions under different solar radiation intensities.

Figure 8 also explains that the compressor input work decreases by 9.0% as the solar radiation intensity grows from 100 to 800 W m^{-2}, which implies that the increment of the overall exergy input is attributable almost entirely to the explosion of the solar energy input.

The system exergy performance of a thermodynamic system is determined by the exergy destructions of the system components, and then the exergy destructions in the main components of the DS-VIHP system are illustrated in **Figure 9**. The solar radiation intensity is selected as 300 and 600 W m^{-2}, when the evaporating temperature is regarded as −20°C and −10°C. As shown in the **Figure 9**, the maximal component irreversibility exists in the solar collector. According to the calculation results, 53.7% and 52.3% of the system exergy input are, respectively, destructed in the solar collector when the evaporating temperature is 20°C and −10°C under the constant solar radiation intensity of 600 W m^{-2}. Meanwhile, under the constant evaporating temperature of −10°C, the exergy destruction in the solar collector will rise by 111.4% (from 934.4 to 1975.6 W) as increasing the solar radiation intensity by 300 W m^{-2}, and the summation of the exergy destructions in all the other components relatively decreases by 2.6%. Therefore, the system exergy efficiency is mainly determined by the irreversibility of the solar collector, and then the system exergy efficiency decreases with enhancing the solar radiation, as shown in **Figure 8**. Meanwhile, it also indicates that the solar collector should yield the highest priority when conducting the component optimization. **Figure 9** also displays that the exergy destructions in the compressor, evaporator, and throttling valve I slightly decrease as it enhances the solar radiation. As shown, the exergy destructions in the compressor, evaporator, and throttling valve I, respectively, reduce by 4.9%, 10.1%, and 59.2% at the evaporating temperature of −10°C, as the G grows by 300 W m^{-2}. Then, the summation of the exergy destructions in all the components except for the solar collector is decreased as the solar radiation intensity improves, although the exergy destructions in the condenser and throttling valve II yield uptrend due to the increase of the intermediate pressure and refrigerant injection ratio. This phenomenon can express the reason for utilizing solar energy benefiting the system heating COP in the perspective of the second law of thermodynamics. In addition, it can be seen from **Figure 9** that the exergy destruction in the solar collector reduces with decreasing the evaporating temperature. It can be mainly attributed to the reduction of the heat leak to ambient, which is resulted from the reduction of the intermediate pressure as decreasing the evaporating pressure.

Aiming to assess the influence of the intermediate pressure on the system irreversibility, the component exergy destructions under different intermediate pressures are illustrated in

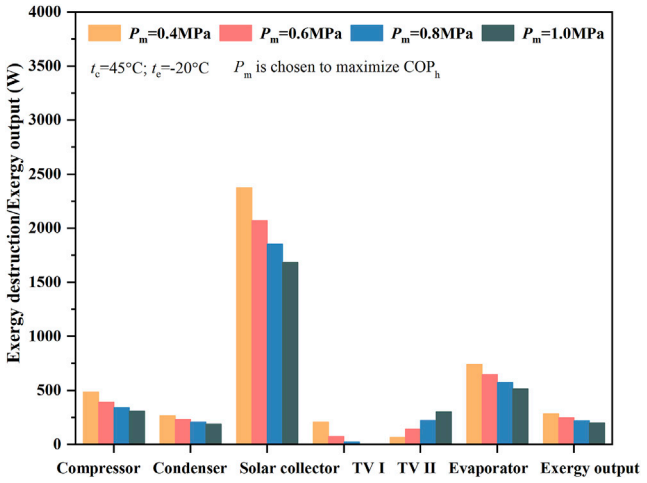

FIGURE 10 | Component exergy destructions under different intermediate pressures.

Figure 10. The condensing temperature and the evaporating temperature are constant at 45°C and −20°C. As shown, except for the throttling valve II, the exergy destructions in other components decrease by lifting the intermediate pressure. The calculation results show that the exergy destructions in the compressor, condenser, solar collector, throttling valve I, and evaporator, respectively, reduce by 36.4%, 28.5%, 29.1%, 97.0%, and 30.8%, by improving the intermediate pressure from 0.4 to 1.0 MPa. The refrigerant vapor quality at the vapor–liquid separator inlet will decrease by lifting the intermediate pressure and further leads to the reduction of the vapor quality at the separator inlet and the injection ratio. Furthermore, the refrigerant flow rates through the compressor, condenser, solar collector, and throttling valve I decrease, which contributes to the exergy destruction reduction in the aforementioned components. The refrigerant vapor quality at the evaporator inlet grows up with raising the intermediate pressure, which brings the refrigerant exergy reduction at the evaporator entrance. Therefore, the exergy destruction in the evaporator yields a reduction tendency, since the refrigerant state at the evaporator outlet remains unchanged. Moreover, **Figure 10** also displays that the system heat exergy output decreases by lifting the intermediate pressure. Actually, by lifting the injection pressure from 0.4 to 1.0 MPa, the heat exergy output decreases by 28.9%, mainly resulting from the reduction of the refrigerant flow rate through the condenser. In addition, it can be seen that the throttling valve II is the unique component whose exergy destruction grows up as the intermediate pressure rises, resulting from the increment of the working pressure differential of the throttling valve II.

Aiming to compare the exergy performance of the two systems, the irreversibility distributions of the DS-VIHP system and the FVHP systems are, respectively, illustrated in **Figures 11A,B**, when the condensing temperature and the evaporating temperature are kept at 45°C and −20°C. The solar radiation intensity is 600 W m^{-2}, and the optimal intermediate pressure for the maximum heating COP is chosen for the two system. It can be seen that the DS-VIHP system can reduce the electricity consumption (W_{com}) by 4.5% (1,624–1,551 W) by utilizing solar energy and improve the heat exergy output (Ex_h) by 20.2% (183.4–220.4 W). Introducing solar energy to increase the ratio of the heat exergy output over the electricity consumption benefits the system's energetic performance. It is worth noting that the exergy destructions in the condenser and throttling valve II of the DS-VIHP system exceed those of the FVHP system. Compared with the FVHP system, the DS-VIHP system owns a large refrigerant flow rate through the condenser, which naturally produces the increment of the exergy destruction in the condenser. The greater irreversibility in the throttling valve II is ascribed to the higher optimal intermediate pressure of the DS-VIHP system (0.808 MPa) over that of the FVHP system (0.456 MPa). Meanwhile, the exergy destructions in the compressor, throttling valve I, and evaporator of the DS-VIHP system are less than those of the FVHP system. Under combined effects of the aforementioned factors, the DS-VIHP system obtains higher exergy output with less electricity consumption

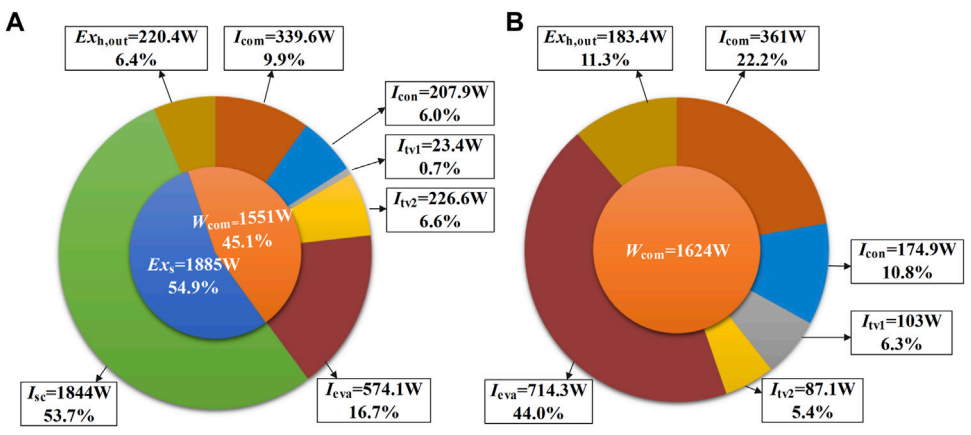

FIGURE 11 | Exergy flow diagrams for the DS-VIHP system **(A)** and the FVHP system **(B)**.

than the FVHP system, which is the motivation for utilizing the solar energy.

CONCLUSION

A novel solar-air dual-source vapor injection heat pump air-conditioner for the electric bus is proposed, which couples the solar energy utilization technique and vapor injection technique to enhance the system heating performance. Three working modes are designed for this proposed system, solar-air dual-source heating mode, air source heating mode, and cooling mode. The heating performance of the proposed system and the conventional vapor injection system is compared based on the built mathematical model, in terms of energetic and exergy aspects. Based on the analysis results, the following conclusions can be obtained:

(1) The proposed system outperforms the conventional system in the heating capacity and COP aspects by 23.2%~12.0% and 30.4%~14.2% under the considered condition, respectively.
(2) Both the proposed system and the conventional system possess the optimal intermediate pressures to achieve the maximal heating COP.
(3) The dual-source mode is preferred for the proposed system under most solar radiation situations, while the air source mode is suitable for the extremely low or no solar radiation situation.
(4) As the solar radiation intensity increases by 700 W m^{-2}, the heat exergy output of the DS-VIHP system increases by 15.5%, but the exergy efficiency decreases by 46.7% due to the rapidly increasing exergy destruction in the solar collector.
(5) Introducing the solar energy in the proposed system increases the heat exergy output and decreases the electricity consumption, compared with the conventional system.

DATA AVAILABILITY STATEMENT

The original contributions presented in the study are included in the article/Supplementary Material; further inquiries can be directed to the corresponding author.

AUTHOR CONTRIBUTIONS

HZ: Conceptualization, data curation, software, and writing—original draft. QL: Methodology and supervision. LY: Methodology, writing—review and editing.

REFERENCES

Besagni, G., Croci, L., Nesa, R., and Molinaroli, L. (2019). Field Study of a Novel Solar-Assisted Dual-Source Multifunctional Heat Pump. *Renew. Energy* 132, 1185–1215. doi:10.1016/j.renene.2018.08.076

Cai, J., Zhang, F., and Ji, J. (2020). Comparative Analysis of Solar-Air Dual Source Heat Pump System with Different Heat Source Configurations. *Renew. Energy* 150, 191–203. doi:10.1016/j.renene.2019.12.128

Chen, J., and Yu, J. (2018). Energy and Exergy Analysis of a New Direct-Expansion Solar Assisted Vapor Injection Heat Pump Cycle with Subcooler for Water Heater. *Sol. Energy* 171, 613–620. doi:10.1016/j.solener.2018.07.019

Choi, Y. U., Kim, M. S., Kim, G. T., Kim, M., and Kim, M. S. (2017). Performance Analysis of Vapor Injection Heat Pump System for Electric Vehicle in Cold Startup Condition. *Int. J. Refrig.* 80, 24–36. doi:10.1016/j.ijrefrig.2017.04.026

Diez, F. J., Navas-Gracia, L. M., Martínez-Rodríguez, A., Correa-Guimaraes, A., and Chico-Santamarta, L. (2019). Modelling of a Flat-Plate Solar Collector Using Artificial Neural Networks for Different Working Fluid (Water) Flow Rates. *Sol. Energy* 188, 1320–1331. doi:10.1016/j.solener.2019.07.022

Fazhan, P., Mingshan, W., Haisheng, H., and Hong, Z. (2014). Effects of Different Ambient Temperatures on Performance of Electric Vehicles' Heat Pump Air Conditioning. *J. Beijing Univ. Aeronautics Astronautics* 40 (12), 1741–1746. doi:10.13700/j.bh.1001-5965.2013.0754

Feng, L., and Hrnjak, P. (2016). Experimental Study of an Air Conditioning-Heat Pump System for Electric Vehicles. *SAE Int. J. Passen. Car.* 9 (1), 68–74. doi:10.4271/2016-01-0257

Göhlich, D., Ly, T.-A., Kunith, A., and Jefferies, D. (2015). Economic Assessment of Different Air-Conditioning and Heating Systems for Electric City Buses Based on Comprehensive Energetic Simulations. *World Electr. Veh. J.* 7 (3), 398–406. doi:10.3390/wevj7030398

Han, X., Zou, H., Xu, H., Tian, C., and Kang, W. (2019). Experimental Study on Vapor Injection air Source Heat Pump with Internal Heat Exchanger for Electric Bus. *Energy Procedia* 158, 4147–4153. doi:10.1016/j.egypro.2019.01.817

Jafarkazemi, F., and Ahmadifard, E. (2013). Energetic and Exergetic Evaluation of Flat Plate Solar Collectors. *Renew. Energy* 56, 55–63. doi:10.1016/j.renene.2012.10.031

Kim, D., Jeon, Y., Jang, D. S., and Kim, Y. (2018). Performance Comparison Among Two-Phase, Liquid, and Vapor Injection Heat Pumps with a Scroll Compressor Using R410a. *Appl. Therm. Eng.* 137, 193–202. doi:10.1016/j.applthermaleng.2018.03.086

Kwon, C., Kim, M. S., Choi, Y., and Kim, M. S. (2017). Performance Evaluation of a Vapor Injection Heat Pump System for Electric Vehicles. *Int. J. Refrig.* 74, 138–150. doi:10.1016/j.ijrefrig.2016.10.004

Lemmon, E. W., Bell, I. H., Huber, M. L., and McLinden, M. O. (2018). *Nist Standard Reference Database 23: Reference Fluid Thermodynamic and Transport Properties-Refprop*. version 10.0. Retried From. Gaithersburg, MD: National Institute of Standards and Technology.

Li, H.-J., Zhou, G.-H., Li, A.-G., Li, X.-G., Li, Y.-N., and Chen, J. (2014). Heat Pump Air Conditioning System for Pure Electric Vehicle at Ultra-low Temperature. *Therm. Sci.* 18 (5), 1667–1672. doi:10.2298/tsci1405667l

Li, W., Liu, R., Liu, Q., Liu, Y., Wang, D., Xia, S., et al. (2020). Upstream and Downstream Injection Effects on R134a Economized Vapor Injection Heat Pump System at Low Temperatures for Electric Vehicles. *Int. J. Refrig.* 120, 1–11. doi:10.1016/j.ijrefrig.2020.04.003

Li, Y., Shi, J., Cheng, X., and Liang, Z. (2016). *Design and Experiment of Heat Pump Air-Conditioning System for Electric Vehicle*. Refrigeration 35 (02), 18–22. doi:10.3696/J.ISSN.1005-9180.2016.02.004

Llopis, R., Sanz-Kock, C., Cabello, R., Sánchez, D., and Torrella, E. (2015). Experimental Evaluation of an Internal Heat Exchanger in a Co2 Subcritical Refrigeration Cycle with Gas-Cooler. *Appl. Therm. Eng.* 80, 31–41. doi:10.1016/j.applthermaleng.2015.01.040

Peng, Q., and Du, Q. (2016). Progress in Heat Pump Air Conditioning Systems for Electric Vehicles-A Review. *Energies* 9 (4), 240. doi:10.3390/en9040240

Pridasawas, W., and Lundqvist, P. (2004). An Exergy Analysis of a Solar-Driven Ejector Refrigeration System. *Sol. Energy.* 76 (4), 369–379. doi:10.1016/j.solener.2003.11.004

Qin, X., Wang, D., Jin, Z., Wang, J., Zhang, G., and Li, H. (2021). A Comprehensive Investigation on the Effect of Internal Heat Exchanger Based on a Novel Evaluation Method in the Transcritical Co2 Heat Pump System. *Renew. Energy* 178, 574–586. doi:10.1016/j.renene.2021.06.082

Redón, A., Navarro-Peris, E., Pitarch, M., Gonzálvez-Macia, J., and Corberán, J. M. (2014). Analysis and Optimization of Subcritical Two-Stage Vapor Injection Heat Pump Systems. *Appl. Energy* 124, 231–240. doi:10.1016/j.apenergy.2014.02.066

Wang, J., Qv, D., Yao, Y., and Ni, L. (2021). The Difference between Vapor Injection Cycle with Flash Tank and Intermediate Heat Exchanger for Air Source Heat Pump: an Experimental and Theoretical Study. *Energy* 221, 119796. doi:10.1016/j.energy.2021.119796

Wang, Z., Wei, M., Peng, F., Liu, H., Guo, C., and Tian, G. (2016). Experimental Evaluation of an Integrated Electric Vehicle Ac/hp System Operating with R134a and R407c. *Appl. Therm. Eng.* 100, 1179–1188. doi:10.1016/j.applthermaleng.2016.02.064

Wei, W., Ni, L., Xu, L., Yang, Y., and Yao, Y. (2020). Application Characteristics of Variable Refrigerant Flow Heat Pump System with Vapor Injection in Severe Cold Region. *Energy Build.* 211, 109798. doi:10.1016/j.enbuild.2020.109798

Xiao, X., Chen, Z., Wang, C., and Nie, P. (2020). Effect of an Electric Vehicle Promotion Policy on china's Islands: A Case Study of Hainan Island. *Front. Energy Res.* 8, 132. doi:10.3389/fenrg.2020.00132

Zhang, R., Stanke, E. J., Zhang, G., Lu, Y., Sun, X., and Li, X. (2019). Benefits Investigation of Electronic Expansion Valve in Electric Vehicle Thermal System as Compared to Thermal Expansion Valve with Shut-Off Valve. *Int. J. Refrig.* 100, 404–413. doi:10.1016/j.ijrefrig.2019.02.018

Zhang, Z., Wang, J., Feng, X., Chang, L., Chen, Y., and Wang, X. (2018). The Solutions to Electric Vehicle Air Conditioning Systems: a Review. *Renew. Sustain. Energy Rev.* 91, 443–463. doi:10.1016/j.rser.2018.04.005

Conflict of Interest: Authors QL and LY are employed by Yutong Bus Co., Ltd.

The remaining author declares that the research was conducted in the absence of any commercial or financial relationships that could be construed as a potential conflict of interest.

Publisher's Note: All claims expressed in this article are solely those of the authors and do not necessarily represent those of their affiliated organizations, or those of the publisher, the editors, and the reviewers. Any product that may be evaluated in this article, or claim that may be made by its manufacturer, is not guaranteed or endorsed by the publisher.

NOMENCLATURE

Abbreviations

A area, m^2

COP coefficient of performance

d density, kg m^{-3}

Ex exergy rate of fluid, W

G solar radiation intensity, W m^{-2}

GWP global warming potential

h specific enthalpy, J kg^{-1}

I exergy destruction, W

m refrigerant mass flow rate, kg/s

n rotational speed, r min^{-1}

NBP normal boiling point

P pressure, MPa

$Q_{\mathbf{h}}$ heating capacity, kW

s specific entropy, J kg^{-1} K^{-1}

t Celsius temperature, °C

T Kelvin temperature, K

$V_{\mathbf{dis}}$ displacement volume, m^3

U heat loss coefficient

W power input, W

Greek symbol

α injection ratio

ε absorption factor

η efficiency

τ transmissivity

φ exergy destruction percentage

Subscripts

0 reference state

1–9 state points of the refrigerant

c condensing

com compressor

con condenser

crit critical condition

e evaporating

eva evaporator

exh heat exergy

h heating

m intermediate

pl plate

sc solar collector

sys system

tv throttling valve

v volumetric